CERN-STUDENTS-Note-2023-094

25 August 2023
vincent.tee.ming.han@cern.ch

Jet phenomenology in simulated proton-proton collisions at $\sqrt{s} = 13.6$ TeV

Vincent Tee Ming Han
CERN, CH-1211 Geneva, Switzerland

Supervised by: Mike Sas, Nima Zardoshti

Keywords: Jet phenomenology, pp collisions, QCD dijet, radius dependence

Summary

This summer student report presents a study of jet phenomenology in simulated proton-proton collisions at $\sqrt{s} = 13.6$ TeV. The QCD dijet events are simulated using PYTHIA 8. The jets are clustered using the anti-k_t algorithm with $R = 0.2$, 0.4, 0.6, and 0.8. The relationship between partons and jets is studied. The R-dependence of jet observables are also investigated.

Contents

1 Introduction

Quarks and gluons are the only known particles that interact through the strong force. However, it is impossible to detect quarks and gluons as a single particle in an experiment. Instead, a quark or gluon experiences fragmentation immediately after creation, resulting in a jet, which is a collimated spray of energetic hadrons [10].

Jets are used extensively in physics experiments. For example, jets are used as a hard probe of the quark-gluon plasma (QGP) in heavy-ion collisions [1, 8, 2]. It is also useful in studying quantum chromodynamics (QCD) [4] and exploring physics beyond the Standard Model [11] in proton-proton (pp) collisions.

Therefore, it is crucial to understand jets properly. In an experiment, jets are defined by jet clustering algorithms. The anti-k_t clustering algorithm [6] is used in this project. In this algorithm, a radius parameter, R, has to be specified. It physically represents the maximum distance in the pseudorapidity η and azimuthal angle ϕ space, $\Delta R = \sqrt{\Delta\eta^2 + \Delta\phi^2}$ that a particle can be clustered into a jet.

By having well-defined jets, one can then utilize them for physics analyses. A jet itself possesses different observables to be studied. Most of these observables depend, inevitably, on the value of R. In this project, the R-dependence of different jet observables, including jet width, and inclusive differential jet cross section are studied in pp collisions at centre-of-mass energy, $\sqrt{s} = 13.6$ TeV. The relationship between jets and partons, along with the effects of multiparton interactions (MPI), initial-state radiation (ISR) and final-state radiation (FSR) on jets are also studied in this project.

2 Simulated samples

Monte Carlo (MC) simulation is used to generate pp collision events at $\sqrt{s} = 13.6$ TeV. Specifically, PYTHIA 8 [5] is used to generate QCD dijet events in minimum bias (MB) setting. MPI, ISR, and FSR are turned on and off for the study of their effects.

3 Jet clustering and matching

The jets are clustered using the anti-k_t algorithm with the FastJet package [6, 7]. E-scheme recombination is used, in which the four-vector of a jet is defined as the sum of the four-vector of its constituents.

The anti-k_t algorithm is a sequential clustering algorithm which is infrared and collinear (IRC) safe. It generally starts its clustering with the hardest objects at every iteration. It then combines the hard objects with the soft objects around them. Therefore, the clustered jets have cone-like jet areas, which are dependent on the value of the radius parameter, R.

In this study, the jets are clustered with $R = 0.2$, 0.4, 0.6, and 0.8. A final-state particle can only be clustered into a jet if its $p_T > 150$ MeV and $|\eta| < 2.0$. All the jets are required to have $|\eta| < 2 - R$.

In order to study how well a jet can represent a parton, they have to be matched to each other. In this project, a jet is said to be matched to a parton if the η-ϕ space distance, ΔR between them is smaller than 0.2.

4 Relationship between partons and jets

One way to study the relationship between partons and jets is to compare their p_T. Figure 1 quantifies the difference in p_T of a parton and its matched jet by their ratio, $p_{T,Jet}/p_{T,Parton}$. The larger the value of R, the higher the ratio, because a jet with a larger R can capture more particles from the parton. When p_T increases, the jets are more collimated, and hence $\mu_{p_{T,Jet}/p_{T,Parton}}$ of all jets starts approaching unity. With MPI, ISR, and FSR turned on, the jets are contaminated with particles originating from these effects, and hence they have a generally higher $\mu_{p_{T,Jet}/p_{T,Parton}}$. The larger the value of R, the more a jet is susceptible to their effects.

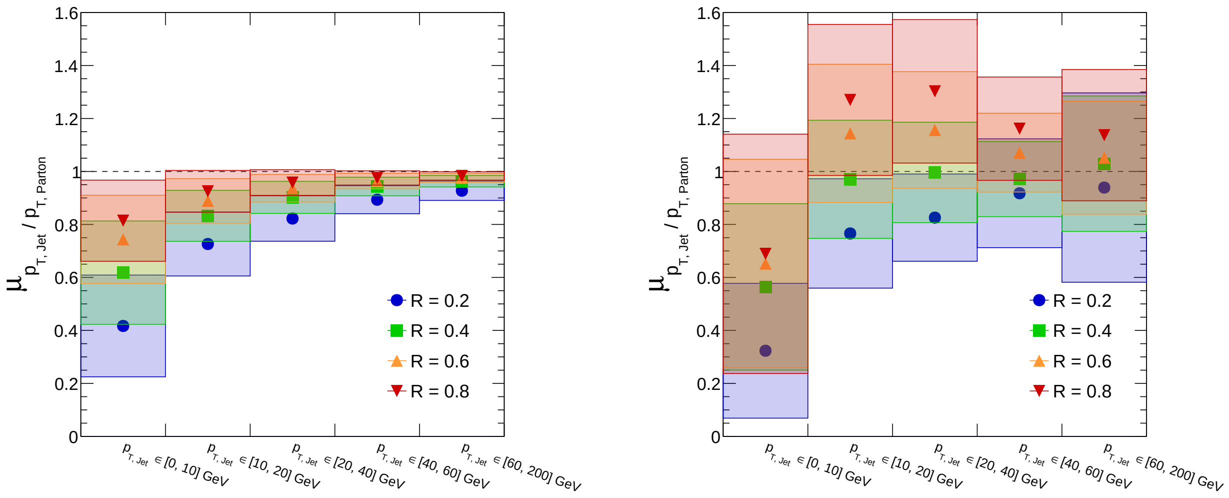

(a) (b)

Figure 1: Gaussian mean of the ratio of $p_{T,Jet}$ to $p_{T,Parton}$ as a function of $p_{T,Jet}$ (a) without (b) with MPI, ISR and FSR. The error bars represent the σ values of the fitted Gaussian distributions.

Figure 2 shows the percentage change in $p_{T,Jet}$ when R is increased by 0.2. When MPI, ISR and FSR are turned off, the increment in p_T is much smaller for jets with larger R. This is because the particles in a jet are concentrated at the core of the jet. However, when all the effects are turned on, the percentage increase in p_T for jets with larger R becomes significantly greater. This is due to the increasing amount of contamination as R increases. As p_T becomes higher, the jets become more collimated, and hence the increment in p_T becomes smaller.

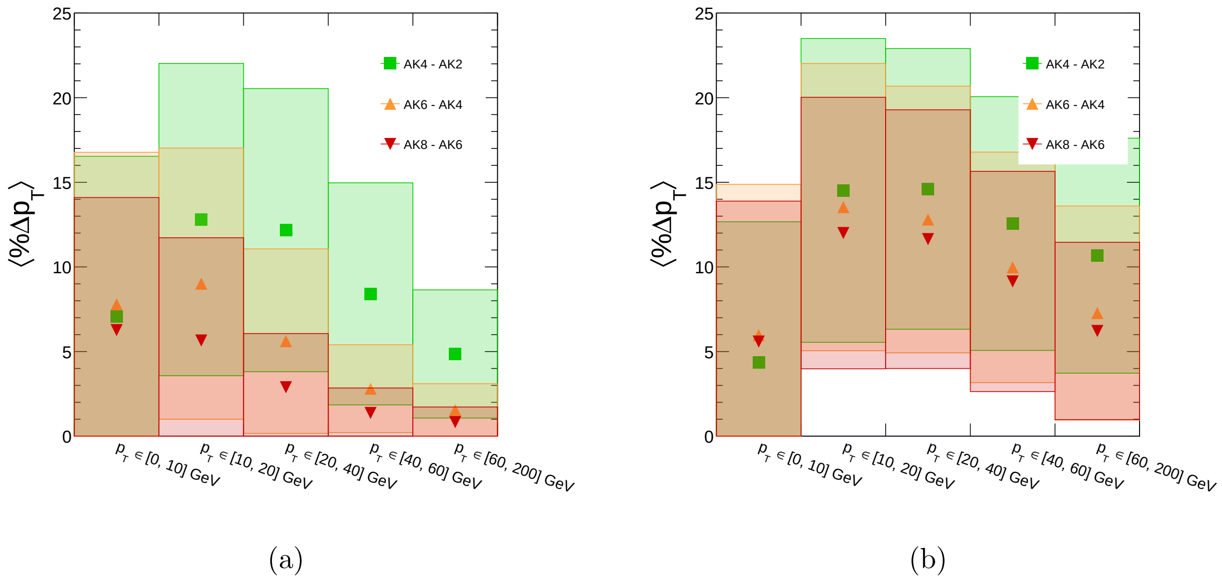

Figure 2: Percentage change in $p_{T,Jet}$ when R is increased by 0.2 (a) without (b) with MPI, ISR and FSR.

5 Jet spectra

There are various jet observables that are dependent on R. For instance, the inclusive differential jet cross section [3]. It is presented in Figure 3 as a case when MPI, ISR and FSR are turned off. As observed, the cross section of jets with larger R is generally higher. However, as p_T increases, the jets become more collimated, and hence the ratio between jets of different R starts to converge.

When MPI, ISR and FSR are turned on, Figure 4 shows the same collimating effect. The ratio between jets of different R becomes significantly larger due to the contamination. By comparing the plot with all jets and the plot with matched jets, it can be seen that the jets with larger R have more "fake" jets. It is an indication that jets with larger R are more susceptible to the background effects. However, as p_T increases, the influence of the contamination becomes lesser, and the two spectra start to look similar.

6 Summary and outlook

This report presents a study of jet phenomenology in simulated pp collisions at $\sqrt{s} = 13.6$ TeV. Jets with different R are reconstructed and compared. Their relationship with the partons and the R-dependence of jet observables are also studied.

In the future, alternative jet matching methods can be explored. For example, one can match a jet with a parton if it contains certain percentage of the parton p_T. R-dependence of jet substructure can also be studied.

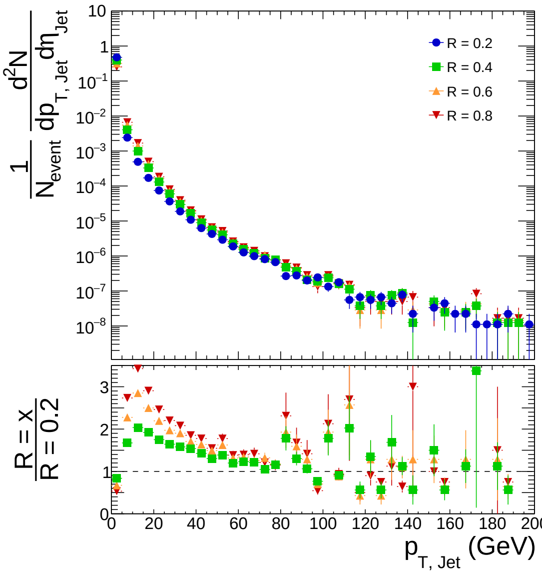

(a)

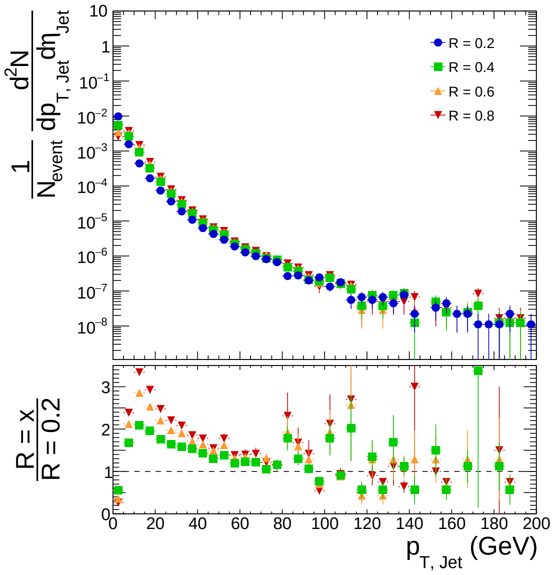

(b)

Figure 3: The upper panel shows the inclusive differential jet cross section for (a) all jets (b) matched jets with $R = 0.2$, 0.4, 0.6, and 0.8. The lower panels represent the ratio of jets with $R = 0.4$, 0.6, and 0.8 to $R = 0.2$. MPI, ISR, and FSR are turned off.

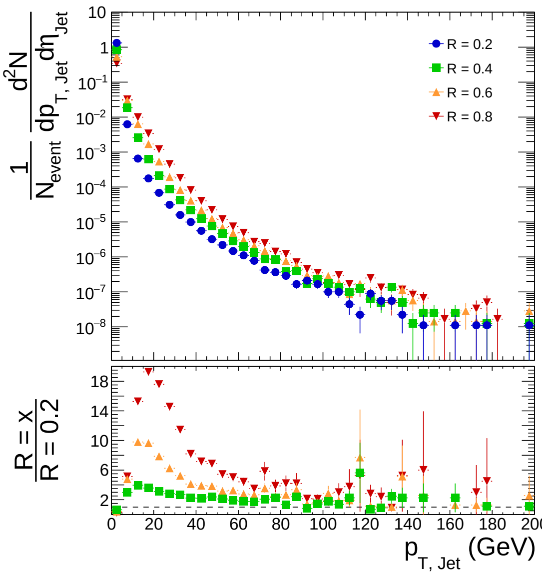

(a)

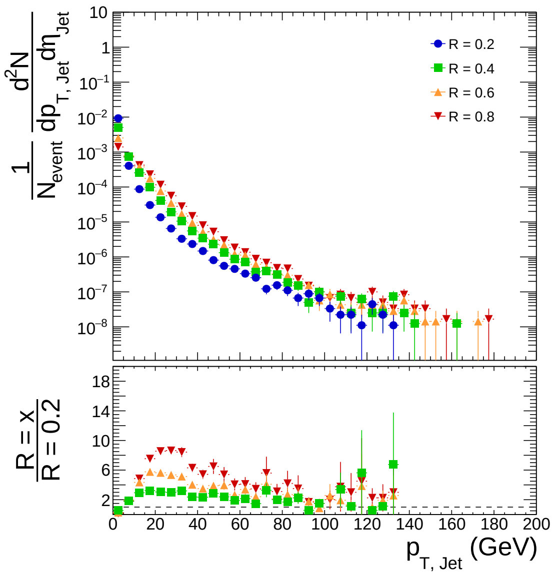

(b)

Figure 4: The upper panel shows the inclusive differential jet cross section for (a) all jets (b) matched jets with $R = 0.2$, 0.4, 0.6, and 0.8. The lower panels represent the ratio of jets with $R = 0.4$, 0.6, and 0.8 to $R = 0.2$. MPI, ISR, and FSR are turned on.

Appendix A Hard QCD events

As a complement to the minimum bias events, hard QCD events are also generated and studied. The results are documented in the following figures. Firstly, hard QCD events with PtHatMin = 40 GeV are generated. Figure 5 shows the arithmetic mean of the η-ϕ space distance, ΔR between a parton and the nearest matched jet axis as a function of $p_{T,Jet}$. Figure 6 shows the Gaussian mean of the ratio of $p_{T,Jet}$ to $p_{T,Parton}$ as a function of $p_{T,Jet}$. Figure 7 presents the percentage change in $p_{T,Jet}$ when R is increased by 0.2. Figure 8 shows the arithmetic mean of the width, $\langle\lambda_1^1\rangle$ of matched jets with different R as a function of $p_{T,Jet}$. Figure 9 shows the correlation matrices of jet width and $\frac{p_{T,Jet}}{p_{T,Parton}}$.

Events with PtHatMin = 100 GeV and PtHatMax = 101 GeV are also generated. Figure 10 shows the jet spectra when MPI, ISR, and FSR are turned off, meanwhile Figure 11 shows the jet spectra when MPI, ISR, and FSR are turned on.

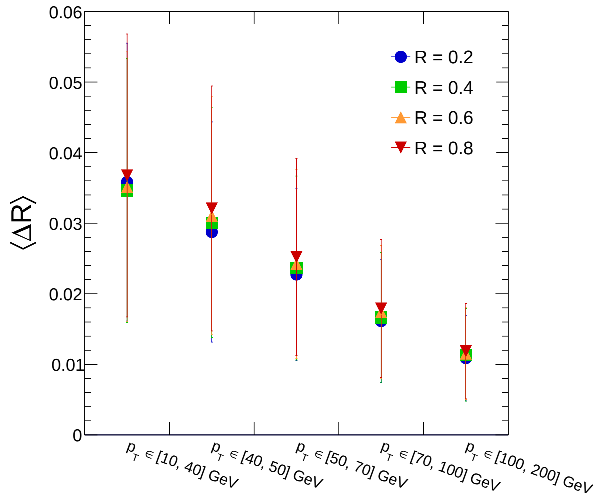

Figure 5: Arithmetic mean of the η-ϕ space distance, ΔR between a parton and the nearest matched jet axis as a function of $p_{T,Jet}$. The error bars represent the RMS values of the distributions. The events are generated with PtHatMin = 40 GeV without MPI, ISR and FSR.

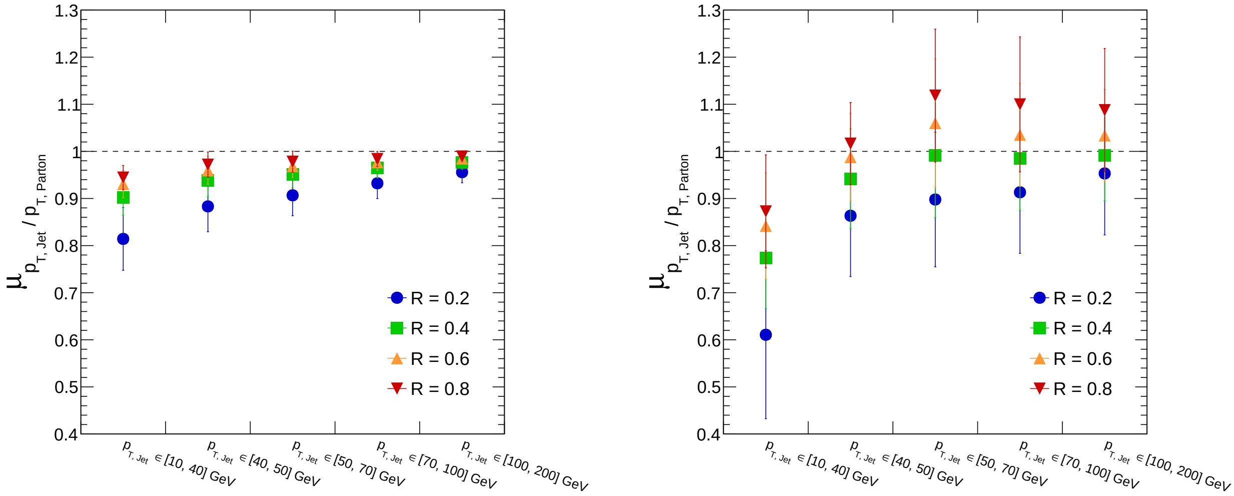

(a) (b)

Figure 6: Gaussian mean of the ratio of $p_{T,Jet}$ to $p_{T,Parton}$ as a function of $p_{T,Jet}$ (a) without (b) with MPI, ISR and FSR. The error bars represent the σ values of the fitted Gaussian distributions. The events are generated with PtHatMin = 40 GeV.

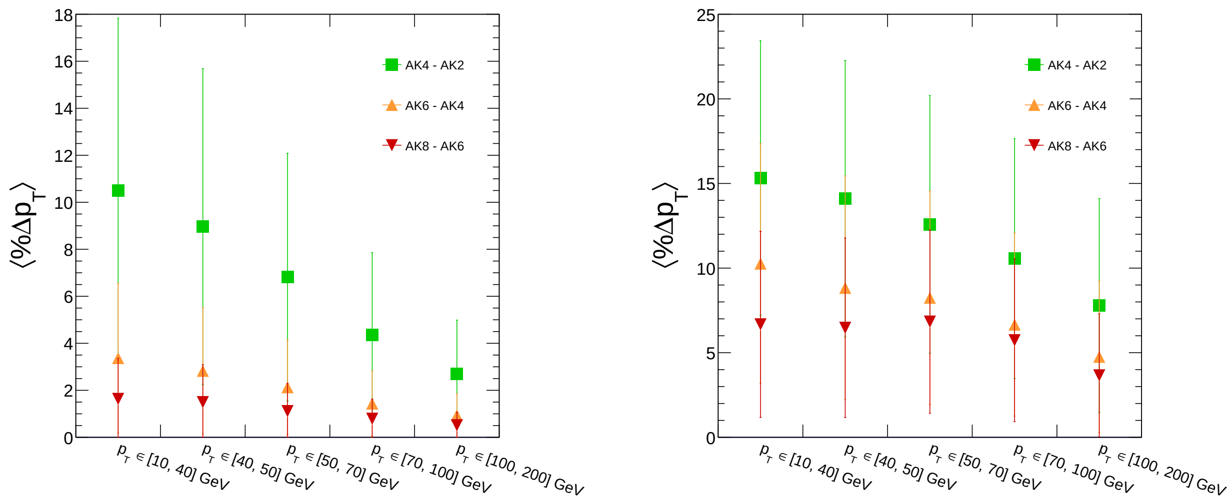

(a) (b)

Figure 7: Percentage change in $p_{T,Jet}$ when R is increased by 0.2 (a) without (b) with MPI, ISR and FSR. The events are generated with PtHatMin = 40 GeV.

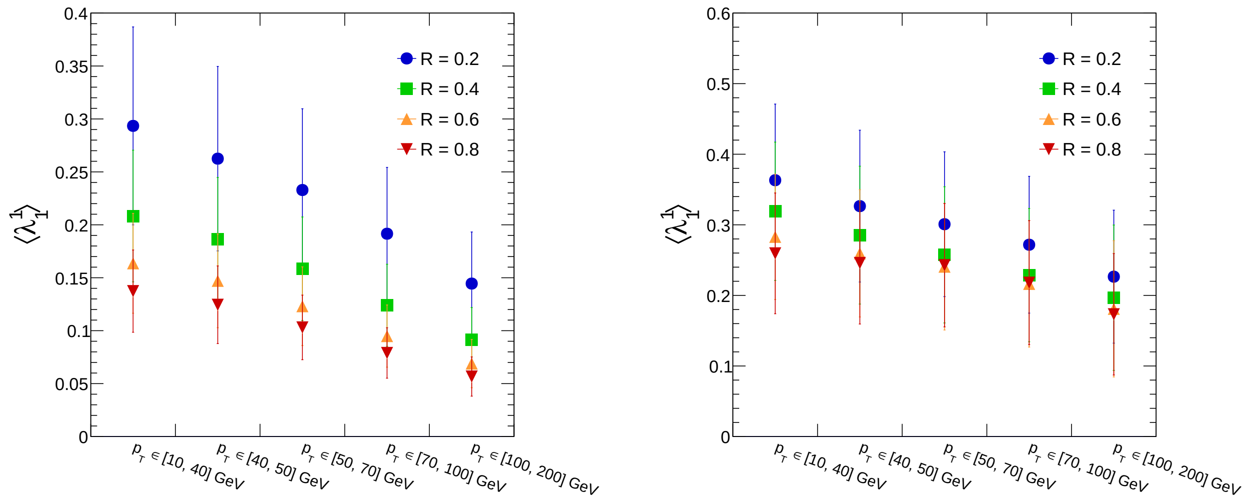

(a) (b)

Figure 8: Arithmetic mean of the width, $\langle \lambda_1^1 \rangle$ [9] of matched jets with different R as a function of $p_{T,Jet}$ (a) without (b) with MPI, ISR and FSR. The error bars represent the RMS values of the distributions. The events are generated with PtHatMin = 40 GeV.

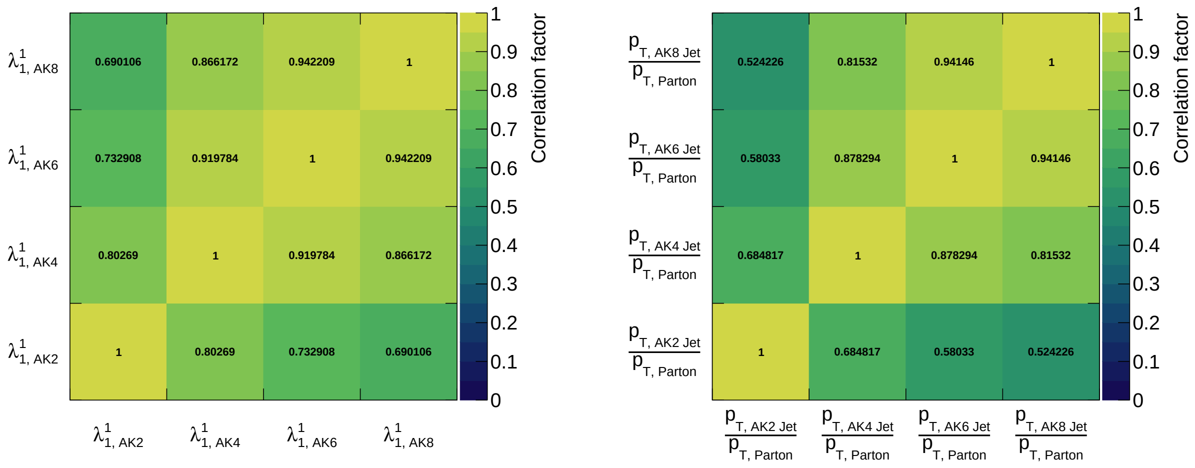

(a) (b)

Figure 9: Correlation matrices to show the correlations of (a) jet width, λ_1^1 and (b) $\frac{p_{T,Jet}}{p_{T,Parton}}$ between jets with different R. The events are generated with PtHatMin = 40 GeV without MPI, ISR and FSR.

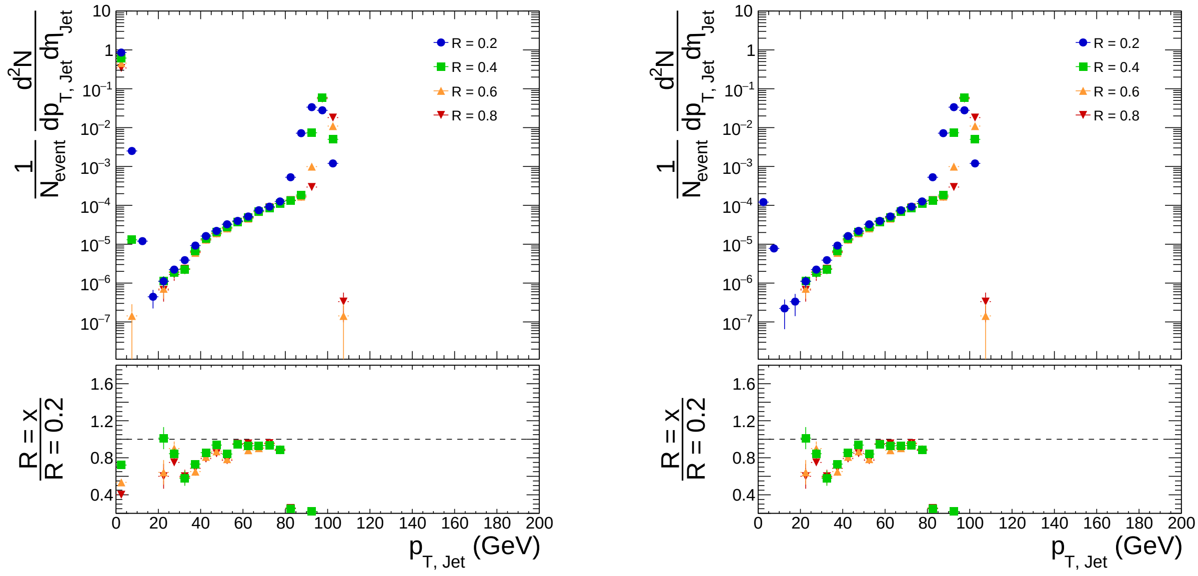

(a) (b)

Figure 10: Jet spectra of (a) all jets (b) matched jets for hard QCD events generated with PtHatMin = 100 GeV and PtHatMax = 101 GeV. MPI, ISR, and FSR are turned off.

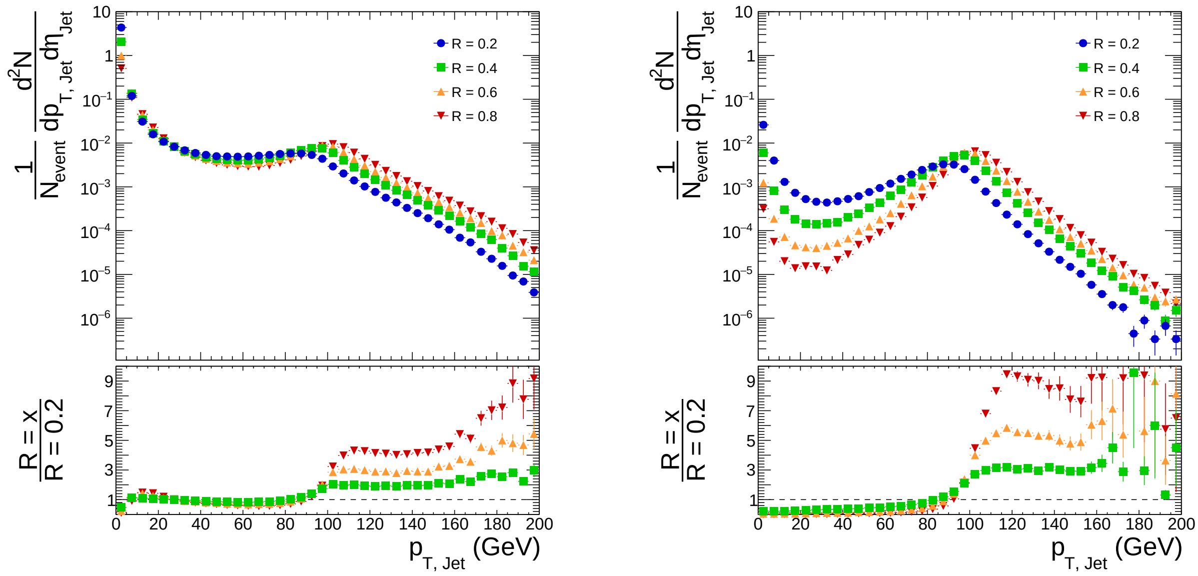

(a) (b)

Figure 11: Jet spectra of (a) all jets (b) matched jets for hard QCD events generated with PtHatMin = 100 GeV and PtHatMax = 101 GeV. MPI, ISR, and FSR are turned on.

Appendix B p_T matching

As an alternative, a jet can be matched to a parton if it contains 50% of the parton p_T. The matched jet spectra obtained with this approach are shown in Figure 12 and Figure 13.

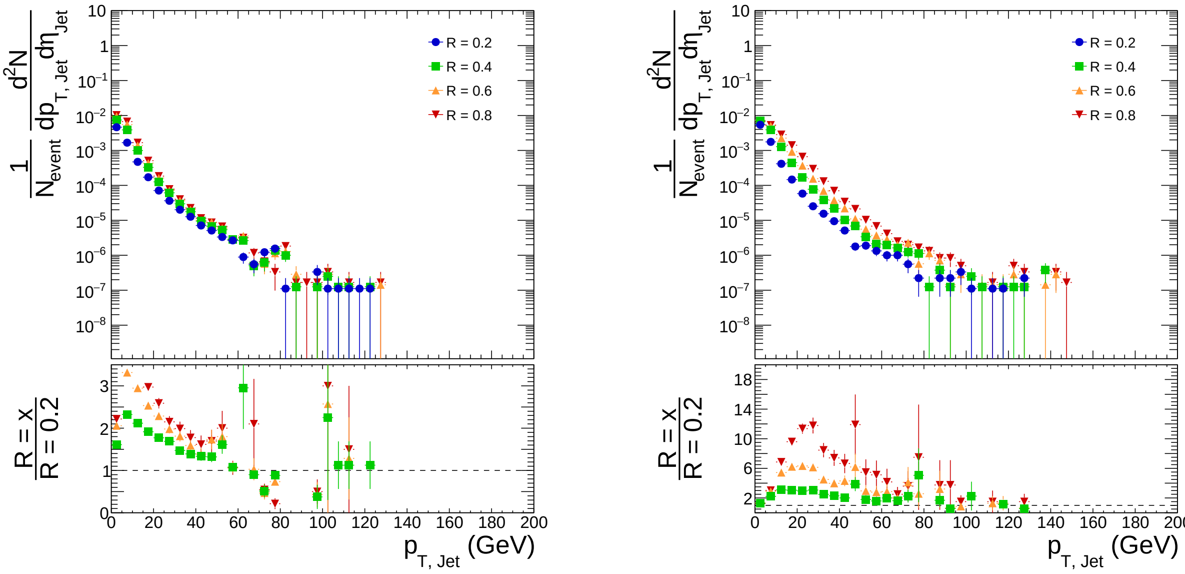

(a) (b)

Figure 12: Matched jet spectra for MB events (a) without (b) with MPI, ISR, and FSR.

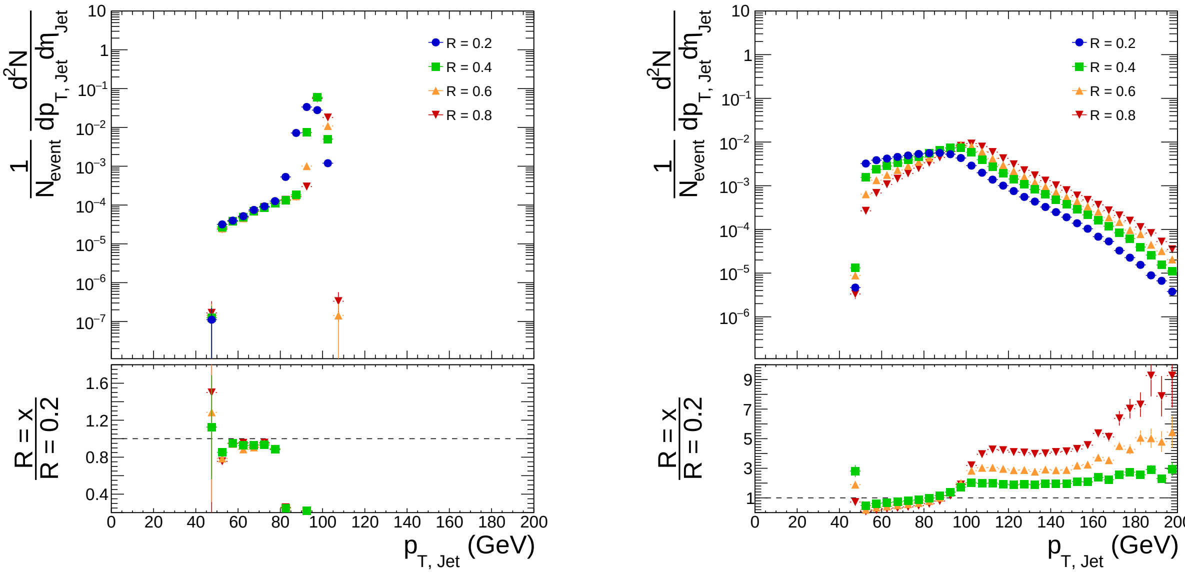

(a) (b)

Figure 13: Matched jet spectra for hard QCD events generated with PtHatMin = 100 GeV and PtHatMax = 101 GeV (a) without (b) with MPI, ISR, and FSR.

Code

All the code of this project is documented in Summer-Project-JETS.

References

[1] The ALICE experiment – A journey through QCD. November 2022.

[2] Measurement of the radius dependence of charged-particle jet suppression in Pb–Pb collisions at $\sqrt{s_{\mathrm{NN}}} = 5.02$ TeV. Technical report, CERN, Geneva, 2023.

[3] B. Abelev et al. Measurement of the inclusive differential jet cross section in *pp* collisions at $\sqrt{s} = 2.76$ TeV. *Phys. Lett. B*, 722:262–272, 2013.

[4] S. Acharya et al. Direct observation of the dead-cone effect in quantum chromodynamics. *Nature*, 605(7910):440–446, 2022.

[5] Christian Bierlich et al. A comprehensive guide to the physics and usage of PYTHIA 8.3. March 2022.

[6] Matteo Cacciari, Gavin P. Salam, and Gregory Soyez. The anti-k_t jet clustering algorithm. *JHEP*, 04:063, 2008.

[7] Matteo Cacciari, Gavin P. Salam, and Gregory Soyez. FastJet User Manual. *Eur. Phys. J. C*, 72:1896, 2012.

[8] Leticia Cunqueiro and Anne M. Sickles. Studying the QGP with Jets at the LHC and RHIC. *Prog. Part. Nucl. Phys.*, 124:103940, 2022.

[9] Andrew J. Larkoski, Jesse Thaler, and Wouter J. Waalewijn. Gaining (Mutual) Information about Quark/Gluon Discrimination. *JHEP*, 11:129, 2014.

[10] Gavin P. Salam. Towards Jetography. *Eur. Phys. J. C*, 67:637–686, 2010.

[11] Armen Tumasyan et al. Search for new heavy resonances decaying to WW, WZ, ZZ, WH, or ZH boson pairs in the all-jets final state in proton-proton collisions at $\sqrt{s} = 13$ TeV. *Phys. Lett. B*, 844:137813, 2023.